HHS Public Access

Author manuscript

Analyst. Author manuscript; available in PMC 2023 July 12.

Published in final edited form as:

Analyst. ; 147(14): 3340–3349. doi:10.1039/d2an00794k.

Ultra-high SERS Detection of Consumable Coloring Agents Using Plasmonic Gold Nanostars with High Aspect-ratio Spikes

Supriya Atta[a,b], **Tongchatra Watcharawittayakul**[a,b], **Tuan Vo-Dinh**[a,b,c,*]

[a]Fitzpatrick Institute for Photonics, Durham, NC 27708, USA

[b]Department of Biomedical Engineering, Durham, NC 27708, USA

[c]Department of Chemistry, Duke University, Durham, NC 27708, USA

Abstract

Solution-based SERS detection by using a portable Raman instrument has emerged as an important tool due to its simplicity, and flexibility for rapid and on-site screening of analyte molecules. However, this method has several shortcomings, including poor sensitivity especially for weak-affinity analyte molecules, where there is no close contact between the plasmonic metal surface and analyte molecule. Examples of weak-affinity molecules include pigment molecules that are commonly used as a consumable coloring agent, such as allura red (AR), and sunset yellow (SY). As high consumption of colorant agents has been shown to cause adverse effects on human health, there is a strong need to develop a simple and practical sensing system with high sensitivity for these agents. Here we present a novel, highly sensitive solution-based SERS detection method for AR, and SY by using CTAC capped gold nanostars (GNS) having different aspect ratios (GNS-2, GNS-4, and GNS-5) without utilizing any aggregating agents which can enhance SERS signal however it reduces batch to batch reproducibility. The influence of the aspect ratio of GNS on SERS properties was investigated. We have achieved a limit of detection (LOD) of AR and SY as low as 0.5 and 1 ppb, respectively by using GNS-5 with the advantages of minimal sample preparation by just mixing the analyte solution into a well plate containing GNS solution. In addition, excellent colloidal stability and reproducibility have further enhanced the applicability in real-world samples. Overall, our results evidence that the solution-based SERS detection platform using high aspect-ratio GNS can be applied for practical application to detect pigment molecules in real samples with satisfactory results.

[*]Corresponding Author, Tuan Vo-Dinh, PhD Director, Fitzpatrick Institute for Photonics R. Eugene and Susie E. Goodson Professor of Biomedical Engineering Professor of Chemistry Duke University Durham, NC 27708, USA, tuan.vodinh@duke.edu.

Author Contributions

The experimental protocol was designed by SA and TV. The experiments were performed by SA and TW the manuscript was first written by SA and revised by TV. All authors have given approval to the final version of the manuscript.

Conflicts of interest

There are no conflicts to declare.

Electronic Supplementary Information (ESI) available: [details of any supplementary information available should be included here]. See DOI: 10.1039/x0xx00000x

Introduction

Synthetic azo colorant pigment molecules are illegally used as color additives because of their advantages of low price, excellent tinting, and improved stability for beverages, drinks, candies, and other food additives.[1–4] However, these pigment molecules are serious threats to human health because of their cytotoxicity, carcinogenicity, and hypersensitivity effects as they can decompose into carcinogenic amine materials.[2, 5–7] Therefore, there remains an urgent need for an analytical technique to prevent this food fraud which can offer a sensitive, rapid, and effective detection of these pigment molecules. Traditional methods for the detection of these pigment molecules are high-performance liquid chromatography (HPLC) and mass spectrometry (MS).[8–10] However, these techniques are time-consuming and require costly instrumentation and special expertise to operate. Therefore, it is highly desirable to develop a cost-effective analytical method that features low cost, minimal sample preparation, high sensitivity, and on-site detection possibility.

Recently, surface-enhanced Raman spectroscopy (SERS) has emerged as a promising analytical tool in different fields including food and drug safety, and environmental monitoring with high sensitivity and selectivity envisioned the molecular fingerprint information of analyte molecules.[11–15] Over three decades our laboratory has been developing different plasmonic-active platforms for a wide variety of applications ranging from SERS chemical sensing to biomedical diagnostics and therapy.[16–19] One main driving force behind this evolution was the discovery of plasmonic noble metal nanoparticles where there occurs an electromagnetic enhancement of Raman signals from molecules in close proximity to plasmonic metal nanoparticles.[20] In addition, the portable feature of the Raman instrument has been developed recently which further enhances its application in the real world. However, despite the widespread use of SERS, their application is still limited, which is mainly because of the poor sensitivity of analyte molecules, especially for weak-affinity analyte molecules like AR, and SY where there is no close contact between the plasmonic metal surface and analyte molecule.[20] To achieve improved sensitivity, most current research has focused on solid substrate-based detection methods. Although these SERS substrates showed highly sensitive detection capabilities, they have some disadvantages including long procedure sample preparation and they are not suitable for rapid and on-site detection. Therefore, it is highly desirable to develop a streamlined SERS sensing platform for on-site detection, involving simple mixing of the analytes with nanoparticle solution and generating an ultra-high SERS signal. In particular, solution-based SERS detection could be a potential platform for rapid and on-site detection as it requires minimal sample preparation.[21, 22] The detection limit of this method, however, is very poor, which further restricts the applicability of solution-based SERS detection. It is reported that the SERS signal can improve by aggregation of nanoparticles.[21–24] Unfortunately, this process affects batch-to-batch reproducibility of SERS measurements because of the uncontrolled aggregation of nanoparticles.[25] These limitations can be circumvented by developing a nanoparticle system that can generate ultra-high SERS signal without the addition of salts for weak-affinity analyte molecules.

The SERS enhancement depends on the localized surface plasmon resonance (LSPR) of plasmonic noble metal nanoparticles, which generates a strong local electric field

to enhance the Raman signals of target molecules.[26] Moreover, plasmonic nanoparticles with sharp edges and rough surfaces can further intensify the local electric field name as “hotspots”.[26–28] Therefore, there is a great interest in the scientific community to synthesize anisotropic nanoparticles to enhance the local electric field. Among the various metal nanoparticles reported to date, anisotropic gold nanostars (GNS) promise to be a potential candidate due to their excellent SERS enhancement properties, tunable plasmon resonance, and good stability in ambient conditions.[29–33] Anisotropic GNS is an excellent SERS platform than other nanoparticle systems owing to three reasons. First, GNS has 3D sharp protruding spikes, thereby facilitating the generation of multiple hot spots than other nanoparticle systems such as nanospheres, nanorods, and nanocubes. Second, GNS has greater flexibility for fine-tuning the size and shape of the morphology.[34] Third, the localized surface plasmon resonance (LSPR) of GNS can be tuned from the visible to NIR region.[35–37] Over the past few years, there are several approaches reported in the literature for GNS synthesis[38] for application in different research fields including biology and medicine, sensing, and photocatalysis.[39–45] For example, we first showed experimentally and computationally that the SERS signal was intensified by increasing spike length and branch number.[46] However, further improvements are still needed for fine-tuning the GNS morphology to achieve ultrahigh SERS sensing.

This study is aimed at synthesizing GNS having multibranched pointed tips which can provide a potential ultra-high SERS sensitivity of consumable analytes (Scheme 1). Three different aspect ratios of GNS: GNS-2, GNS-4, and GNS-5 were synthesized via a surfactant-free seed-mediated synthesis and capped with CTAC for better stability of GNS. For these particles, we elucidate the role of brunch number and aspect ratio on SERS enhancement of AR and SY, where we achieve maximum SERS enhancement using GNS-5. This solution-based SERS platform detects AR and SY down to the level of 0.5 and 1 ppb, which is almost 100 times lower than that reported previously.[4, 21] Furthermore, we showed exceptional reproducibility and stability of the GNS-5. Finally, we have applied our SERS detection strategy for monitoring real-life samples which indicate that our method has the advantages of being convenient, efficient, and highly selective for the detection of AR, and SY which could be very significant for food safety.

Experimental section

Materials and Characterization

Chloroauric acid ($HAuCl_4$), L-ascorbic acid, silver nitrate ($AgNO_3$, 99.8%) hydrochloric acid (HCl), and trisodium citrate ($Na_3C_6H_5O_7$) were purchased from Sigma-Aldrich. Milli-Q deionized (DI) water was used throughout the experiment. The morphology of nanostars was characterized by analysis FEI Tecnai G2 Twin transmission electron microscope, and HAADF STEM images and EDS maps were acquired using Aberration Corrected STEM-Thermo Fisher Titan 80–300. UV-vis spectra were recorded using a Shimadzu UV-3600i spectrometer with cuvettes of 1 cm path length at room temperature.

Synthesis of Gold Seeds

12 nm Au seeds were synthesized by following a modified version of our previously reported method.[33] Briefly, 7.5 mL of 1% sodium citrate solution was added to 50 mL of boiling 1 mM $HAuCl_4$ aqueous solution. It kept boiling for an additional 60 min, and the solution turns to a red color; then, it was cooled to room temperature in an ice bath and stored at 2–4 °C which was used further for nanostars synthesis.

Synthesis of CTAC Capped GNS-2, GNS-4, and GNS-5 Gold Nanostars

Surfactant-free GNSs gold nanostars were synthesized following a modified version of our previously reported method.[47] The synthesis procedure for GNS-2 is as following. Briefly, 50 μL of 1 N HCl was added to a solution containing 50 mL of 0.25 mM $HAuCl_4$ and 500 μL of the citrate capped gold seed solution. Then, 250 μL of 3 mM $AgNO_3$ and 250 μL of 100 mM ascorbic acid were added to the solution with 5 second time interval. The solution was stirred for 2 minutes. Then, 10 mL 0.1 M CTAC solution was added to GNS solution and stirred for an hour. The solution was centrifuged at 4000 g for 12 min and dispersed in 500 μL of Milli-Q water so that the concentration was 10 times higher than as synthesized nanostars.

The synthesis procedure for GNS-4 is as following. Briefly, 200 μL of 1 N HCl was added to a solution containing 50 mL of 1 mM $HAuCl_4$ and 500 μL of the citrate capped gold seed solution. Then, 2 mL of 3 mM $AgNO_3$ and 1 mL of 100 mM ascorbic acid were added to the solution with 5 second time interval. The solution was stirred for 2 minutes. Then, 10 mL 0.1 M CTAC solution was added to GNS solution and stirred for an hour. The solution was centrifuged at 4000 g for 12 min and dispersed in 500 μL of Milli-Q water so that the concentration was 10 times higher than as synthesized nanostars.

The synthesis procedure for GNS-5 is as following. Briefly, 300 μL of 1 N HCl was added to a solution containing 50 mL of 1.5 mM $HAuCl_4$ and 500 μL of the citrate capped gold seed solution. Then, 3 mL of 3 mM $AgNO_3$ and 1.5 mL of 100 mM ascorbic acid were added to the solution with 5 second time interval. Then, 10 mL 0.1 M CTAC solution was added to GNS solution and stirred for an hour. The solution was centrifuged at 4000 g for 12 min and dispersed in 500 μL of Milli-Q water so that the concentration was 10 times higher than as synthesized nanostars.

Raman Measurements

The SERS measurement was carried out using a lab built portable system having 785 nm laser source (Rigaku Xantus TM-1 handheld Raman device), a fiber optic probe (InPhotonics RamanProbe), a spectrometer (Princeton Instruments Acton LS 785), and a CCD camera (Princeton Instruments PIXIS: 100BR_eXcelon). Laser power of the Rigaku Xantus TM-1 was set at 150 mW and the CCD camera exposure time was set at 10 s. The SERS measurement was standardized using ethanol. The SERS measurement involves a minimal sample preparation in which 300 μL of the gold nanoparticle solution (3 μL stock solution of GNS + 297 μL of Milli-Q-water) were thoroughly mixed with 3μL of analyte solution in 96 well plate whose bottom was covered with aluminum foil to prevent signal interference from the polypropylene well plate.

Results and discussion

The GNS employed in this study were prepared using the surfactant-free nanostars synthesis method.[47, 48] The surfactant-free stars have many advantages over surfactant-based like cetyltrimethylammonium bromide/chloride (CTAB/ CTAC),[49] or polymers based like Triton-X,[41] poly(vinylpyrrolidone) (PVP)[50] nanostars synthesis. First, the morphology of surfactant-free nanostars can be easily tuned by changing the synthesis parameters including gold salts, seeds, ascorbic acid, $AgNO_3$, and HCl concentration.[33, 48, 51] On the other hand, for surfactant-based nanostars synthesis, the surfactant molecules bind on highly energetic crystal facets of intermediated seeds to stabilize the seeds, thereby generating of a smaller number of nucleation centers to grow the spikes which result in a lower number of spikes.[41] Moreover, the plasmon peak of surfactant-free stars can be easily tuned to the visible to NIR region so that we can utilize the 785 lasers to achieve the highest SERS enhancement.[48]

Synthesis and Stability of GNS

Surfactant-free GNS consists of a spherical core and sharp protruding spikes exposed from the core.[33, 47] The nanostars morphology is formed when gold salts, ascorbic acid, $AgNO_3$, and HCl at an ideal concentration for surfactant-free GNS formation were added to the spherical gold seeds solution. The morphology of the nanostars is highly depended on the concentration of the chemicals including gold salts, ascorbic acid, $AgNO_3$, HCl, and gold seeds.[48, 52, 53] Interestingly, it is reported that the formation and stabilization of the spikes is highly dependent on $AgNO_3$ concentration where a monolayer of silver atoms deposited on the highly energetic gold atoms present on the surface of the spikes and stabilized the spike morphology.[41] In this study, we have synthesized three different aspect ratios of GNS (GNS-2, GNS-4, and GNS-5) by following a modified version of the surfactant-free GNS synthesis method reported previously by our group.[47] The aspect ratio of GNS is the ratio of the spike length and width of the spike at the core of GNS, which is directly correlated to the synthetic parameters of GNS. For example, the GNS-2, and GNS-4 were achieved by simply varying the concentration of Ag^+, and ascorbic acid while keeping all other parameters (gold salts, seeds, and HCl concentration) constant. Whereas the GNS-5 was achieved by increasing the concentration of all the variables: gold salts, seeds, ascorbic acid, $AgNO_3$, and HCl concentration from the concentration of synthetic parameters of GNS-2 and GNS-4. Representative TEM images (Figure 1) revealed that GNS spike length and spike numbers were increased from GNS-2 to GNS-5. The core size, spike length, spike sharpness, and aspect-ratios of the GNSs were summarized in Table 1. We have determined the spike sharpness of GNS by measuring the dimensions of high-resolution TEM images using the software program ImageJ. Figure 1h shows that the three GNSs's UV-vis spectra exhibits a gradual red-shift of the plasmon resonance from 780 nm to 890 nm with increasing the aspect ratio of the spikes from 2 to 5.

The surfactant-free GNSs were further capped with CTAC. The unique structure of long-chain aliphatic CTAC is favorable to trap aromatic molecules via hydrophobic interactions between aromatic benzene rings of the analyte (AR and SY) and aliphatic carbon chain CTAC, and therefore it could be a suitable platform for trapping weak-affinity aromatic pigment analyte molecules, thereby facilitating ultra-sensitive SERS detection.[21, 54] The

plasmon resonance of GNS was around 10 nm red-shifted after CTAC capping (Figure S2). Interestingly, we observed that the GNS-2 was not stable, and the plasmon resonance peak was blue-shifted from 780 to 610 nm after 24 hours (Figure-S3a). Whereas there were no spectral changes observed over time (after 20 days) for GNS-4, and GNS-5 (Figure S3b–3c), indicating good stability of GNS-4, and GNS-5. The TEM images of GNS-4 and GNS-5 after 20 days were further confirmed that the morphology remains same after 20 days of synthesis (Figure S3d–3e). The low stability of GNS-2 might be attributed due to the low Ag content present on the highly energetic spikes, thereby the spikes were shrunk with time and the plasmon resonance was blue-shifted.[41]

SERS Measurement and Reproducibility

To evaluate the SERS sensitivity of GNSs, we employed AR and SY as a SERS analyte. The SERS measurements were performed after 30 minutes of mixing 3 μL of the analyte solution (AR, and SY) with the 297 μL nanostars solution so that the analyte molecules can incorporate into the CTAC bilayer and get closer to the nanostars. The SERS spectra of AR show characteristic peaks at 978, 1130, 1188, 1224, 1272, 1385, 1411, 1500, 1582, and 1611 cm^{-1} which match with the reported result.[4, 21] We have selected the highest intense peak at 1500 cm^{-1} for sensitivity determination, and this band was used to compare the SERS of GNSs. For SY, the characteristic SERS peaks are at 986, 1168, 1228, 1395, 1504, 1598 cm^{-1} and, we have selected 1395 cm^{-1} to determine the sensitivity of GNSs.[21, 55]

We have first investigated the effect of the aspect-ratio of GNS on SERS performance of AR and SY at 500 ppb concentration. As seen from Figure 2a, the SERS signal intensity of AR was 4 times higher for GNS-4 than GNS-2 and 8 times higher for GNS-5 than GNS-2. On the other hand, Figure 2b shows the SERS signal of SY, where the SERS intensity was 8 times higher for GNS-4 than GNS-2 and 11 times higher for GNS-5 than GNS-2. As anticipated, GNS-5 shows higher SERS enhancement than GNS-2 and GNS-4 because of a higher number of spikes present in GNS-5 than GNS-2 and GNS-4 resulting generation of a high number of hot spots, thereby enhancing the SERS signal. It is noteworthy that not only the aspect-ratio, but other parameters (spike number, core size, spike length, spike sharpness) also contribute to the SERS enhancement.

Figures 3a–b, and 3c–d show representative SERS spectra and calibration curve of AR (3a–b) and SY (3c–d) dye using GNS-5 where ten different samples were selected for each concentration of the analytes. The SERS intensity at 1500 cm^{-1} was selected as a function of the AR concentration. The concentration of AR follows a linear relationship with the intensity at 1500 cm^{-1}. The linear equation for AR is $I = 1662 + 108C_{AR}$ where I is the intensity at 1500 cm^{-1} and C_{AR} is the concentration of AR. The concentration of SY also follows a linear relationship with the intensity at 1395 cm^{-1}. The linear equation for SY is $I = 2777 + 46C_{SY}$ where I is the intensity at 1395 cm^{-1} and C_{SY} is the concentration of SY. It is important to notify that the detection limit was achieved by our method is up to 0.1 ppb for AR and 1 ppb for SY, which is at least 100 times lower than the previously reported values without using any aggregating agents.[4, 21] Such significant improvements in detection sensitivity might be attributed to the higher number of “hot spots” present in the GNS-5 than that of gold nanorods or nanospheres.

We have further investigated the reproducibility of SERS measurement of GNS-5 at 500 ppb concentration of AR. Ten different sample spots of GNS-5 were randomly selected. Figure 3e shows the peak intensities at 1500 cm $^{-1}$. The relative standard deviation (RSD) value was 4% indicating high reproducibility for this solution-based SERS detection method. Moreover, we have studied the stability of the substrate for 20 days measured at 5 days interval. Figure 3f shows that the SERS spectrum was identical, indicating higher stability of GNS-5 over 20 days.

Application to Real-Sample Analysis

We have validated our SERS platform to detect trace amounts of AR and SY in practical beverage samples. The beverage sample was purchased from a market. Figure 4 shows the SERS spectra of strawberry juice, fruit juice, and Thai tea samples. The results clearly show the characteristic SERS peaks of AR for strawberry juice, and fruit juice, and SY for Thai tea samples. The concentrations of AR and SY were calculated from the linear equation of AR and SY. The concentration of AR in strawberry juice, and fruit juice was 90.4 and 141.8 ppb, respectively. The concentration of SY in Thai tea sample was 19.9 ppb. Overall, this method demonstrated that the CTAC-capped GNS can be applied for the detection of AR and SY in beverages with ultrahigh sensitivity. We have further performed measurements to demonstrate that our method is capable of monitoring changes with AR concentrations in fruit juice sample by addition of various amounts of AR, where we observed that the intensity of the SERS peak at 1500cm^{-1} was enhanced with increasing concentration of AR from 50 ppb to 400 ppb with fruit juice sample (Figure S4). The detailed investigation to determine the concentrations of the AR, SY, and other food colorants in consumer products using lab-based methods such as HPLC-MS to compare with our SERS results will be considered in further studies.

Conclusions

In conclusion, we demonstrated a simple approach for fabricating high aspect-ratio GNSs with CTAC which was utilized for solution-based SERS detection of weak-affinity molecules like AR and SY. Our SERS measurement platform was streamlined with minimal sample preparation by just mixing the analytes into a well plate with GNS and utilizing a portable Raman instrument for rapid detection. With this method using GNS-5, we have achieved a limit of detection of AR, and SY as low as 0.5 ppb and 1 ppb, respectively. Furthermore, we have validated our method with quantitative analysis of AR and SY in beverages. As the synthesis procedure for high aspect ratio GNSs is easy and they exhibit long-term stability, they can be useful for specific applications in biosensing even in presence of a complex environment.

Supplementary Material

Refer to Web version on PubMed Central for supplementary material.

Acknowledgements

This work is supported by the National Institutes of Health (R01GM135486), the US Department of Energy Office of Science (DE-SC0019393), and the Bill and Melinda Gates Foundation (INV-040790).

We acknowledge that this work is made by using the electron microscopy facilities at Duke, and North Carolina State University.

Notes and references

1. Neng J; Xu K; Wang Y; Jia K; Zhang Q; Sun P, Sensitive and Selective Detection of New Red Colorant Based on Surface-Enhanced Raman Spectroscopy Using Molecularly Imprinted Hydrogels. Applied Sciences 2019, 9 (13).
2. Tsuda S; Murakami M; Matsusaka N; Kano K; Taniguchi K; Sasaki YF, DNA Damage Induced by Red Food Dyes Orally Administered to Pregnant and Male Mice. Toxicological Sciences 2001, 61 (1), 92–99. [PubMed: 11294979]
3. Dinç E; Baydan E; Kanbur M; Onur F, Spectrophotometric multicomponent determination of sunset yellow, tartrazine and allura red in soft drink powder by double divisor-ratio spectra derivative, inverse least-squares and principal component regression methods. Talanta 2002, 58 (3), 579–594. [PubMed: 18968786]
4. Yao Y; Wang W; Tian K; Ingram WM; Cheng J; Qu L; Li H; Han C, Highly reproducible and sensitive silver nanorod array for the rapid detection of Allura Red in candy. Spectrochimica Acta Part A: Molecular and Biomolecular Spectroscopy 2018, 195, 165–171. [PubMed: 29414574]
5. Chung KT, Mutagenicity and carcinogenicity of aromatic amines metabolically produced from Azo Dyes. Journal of Environmental Science and Health, Part C 2000, 18 (1), 51–74.
6. Ashida H; Hashimoto T; Tsuji S; Kanazawa K; Danno G. i., Synergistic Effects of Food Colors on the Toxicity of 3-Amino-1, 4-dimethyl-5*H*-pyrido[4, 3-*b*]indole (Trp-P-1) in Primary Cultured Rat Hepatocytes. Journal of Nutritional Science and Vitaminology 2000, 46 (3), 130–136. [PubMed: 10955279]
7. Rovina K; Siddiquee S; Shaarani SM, Extraction, Analytical and Advanced Methods for Detection of Allura Red AC (E129) in Food and Beverages Products. Frontiers in Microbiology 2016, 7.
8. Qi P; Lin Z.-h.; Chen G.-y.; Xiao J; Liang Z.-a.; Luo L.-n.; Zhou J; Zhang X.-w., Fast and simultaneous determination of eleven synthetic color additives in flour and meat products by liquid chromatography coupled with diode-array detector and tandem mass spectrometry. Food Chemistry 2015, 181, 101–110. [PubMed: 25794727]
9. Yu Y; Fan Z, Magnetic solid-phase extraction coupled with HPLC for the determination of Allura Red in food and beverage samples. Food Additives & Contaminants: Part A 2016, 33 (10), 1527–1534.
10. Müller-Maatsch J; Schweiggert RM; Carle R, Adulteration of anthocyanin- and betalain-based coloring foodstuffs with the textile dye 'Reactive Red 195' and its detection by spectrophotometric, chromatic and HPLC-PDA-MS/MS analyses. Food Control 2016, 70, 333–338.
11. Jiang L; Hassan MM; Ali S; Li H; Sheng R; Chen Q, Evolving trends in SERS-based techniques for food quality and safety: A review. Trends in Food Science & Technology 2021, 112, 225–240.
12. Ai Y.-j.; Liang P; Wu Y.-x.; Dong Q.-m.; Li J.-b.; Bai Y; Xu B-J; Yu Z; Ni D, Rapid qualitative and quantitative determination of food colorants by both Raman spectra and Surface-enhanced Raman Scattering (SERS). Food Chemistry 2018, 241, 427–433. [PubMed: 28958550]
13. Gukowsky JC; Xie T; Gao S; Qu Y; He L, Rapid identification of artificial and natural food colorants with surface enhanced Raman spectroscopy. Food Control 2018, 92, 267–275.
14. Barveen NR; Wang T-J; Chang Y-H; Yuan-Liu Z, Ultrasensitive and reusable SERS probe for the detection of synthetic dyes in food industry through hybrid flower-shaped ZnO@Ag nanostructures. Journal of Alloys and Compounds 2021, 861, 157952.
15. Chen C; Liu W; Tian S; Hong T, Novel Surface-Enhanced Raman Spectroscopy Techniques for DNA, Protein and Drug Detection. Sensors (Basel) 2019, 19 (7), 1712. [PubMed: 30974797]
16. Yan F; Wabuyele MB; Griffin GD; Vass AA; Tuan V-D, Surface-enhanced Raman scattering detection of chemical and biological agent simulants. IEEE Sensors Journal 2005, 5 (4), 665–670.
17. Liu Y; Chang Z; Yuan H; Fales AM; Vo-Dinh T, Quintuple-modality (SERS-MRI-CT-TPL-PTT) plasmonic nanoprobe for theranostics. Nanoscale 2013, 5 (24), 12126–12131. [PubMed: 24162005]

18. Liu Y; Maccarini P; Palmer GM; Etienne W; Zhao Y; Lee C-T; Ma X; Inman BA; Vo-Dinh T, Synergistic Immuno Photothermal Nanotherapy (SYMPHONY) for the Treatment of Unresectable and Metastatic Cancers. Scientific Reports 2017, 7 (1), 8606. [PubMed: 28819209]
19. Vo-Dinh T, Surface-enhanced Raman spectroscopy using metallic nanostructures1The submitted manuscript has been authored by a contractor of the U.S Government under contract No. DE-AC05–96OR22464. Accordingly, the U.S. Government retains a nonexclusive, royalty-free license to publish or reproduce the published form of this contribution, or allow others to do so, for U.S. Government purposes.1. TrAC Trends in Analytical Chemistry 1998, 17 (8), 557–582.
20. He H; Li P; Tang X; Lin D; Xie A; Shen Y; Yang L, Developing cysteamine-modified SERS substrate for detection of acidic pigment with weak surface affinity. Spectrochimica Acta Part A: Molecular and Biomolecular Spectroscopy 2019, 212, 293–299. [PubMed: 30660061]
21. Ou Y; Wang X; Lai K; Huang Y; Rasco BA; Fan Y, Gold Nanorods as Surface-Enhanced Raman Spectroscopy Substrates for Rapid and Sensitive Analysis of Allura Red and Sunset Yellow in Beverages. Journal of Agricultural and Food Chemistry 2018, 66 (11), 2954–2961. [PubMed: 29489346]
22. Amin MU; Zhang R; Li L; You H; Fang J, Solution-Based SERS Detection of Weak Surficial Affinity Molecules Using Cysteamine-Modified Au Bipyramids. Analytical Chemistry 2021, 93 (21), 7657–7664. [PubMed: 34013734]
23. Wang H; Xue Z; Wu Y; Gilmore J; Wang L; Fabris L, Rapid SERS Quantification of Trace Fentanyl Laced in Recreational Drugs with a Portable Raman Module. Analytical Chemistry 2021, 93 (27), 9373–9382. [PubMed: 34191499]
24. Sun L; Song Y; Wang L; Guo C; Sun Y; Liu Z; Li Z, Ethanol-Induced Formation of Silver Nanoparticle Aggregates for Highly Active SERS Substrates and Application in DNA Detection. The Journal of Physical Chemistry C 2008, 112 (5), 1415–1422.
25. Laurence TA; Braun G; Talley C; Schwartzberg A; Moskovits M; Reich N; Huser T, Rapid, Solution-Based Characterization of Optimized SERS Nanoparticle Substrates. Journal of the American Chemical Society 2009, 131 (1), 162–169. [PubMed: 19063599]
26. Langer J; Jimenez de Aberasturi D; Aizpurua J; Alvarez-Puebla RA; Auguié B; Baumberg JJ; Bazan GC; Bell SEJ; Boisen A; Brolo AG; Choo J; Cialla-May D; Deckert V; Fabris L; Faulds K; García de Abajo FJ; Goodacre R; Graham D; Haes AJ; Haynes CL; Huck C; Itoh T; Käll M; Kneipp J; Kotov NA; Kuang H; Le Ru EC; Lee HK; Li J-F; Ling XY; Maier SA; Mayerhöfer T; Moskovits M; Murakoshi K; Nam J-M; Nie S; Ozaki Y; Pastoriza-Santos I; Perez-Juste J; Popp J; Pucci A; Reich S; Ren B; Schatz GC; Shegai T; Schlücker S; Tay L-L; Thomas KG; Tian Z-Q; Van Duyne RP; Vo-Dinh T; Wang Y; Willets KA; Xu C; Xu H; Xu Y; Yamamoto YS; Zhao B; Liz-Marzán LM, Present and Future of Surface-Enhanced Raman Scattering. ACS Nano 2020, 14 (1), 28–117. [PubMed: 31478375]
27. Hrelescu C; Sau TK; Rogach AL; Jäckel F; Laurent G; Douillard L; Charra F, Selective Excitation of Individual Plasmonic Hotspots at the Tips of Single Gold Nanostars. Nano Letters 2011, 11 (2), 402–407. [PubMed: 21244014]
28. Shiohara A; Novikov SM; Solís DM; Taboada JM; Obelleiro F; Liz-Marzán LM, Plasmon Modes and Hot Spots in Gold Nanostar–Satellite Clusters. The Journal of Physical Chemistry C 2015, 119 (20), 10836–10843.
29. Fabris L, Gold Nanostars in Biology and Medicine: Understanding Physicochemical Properties to Broaden Applicability. The Journal of Physical Chemistry C 2020, 124 (49), 26540–26553.
30. Guarino-Hotz M; Allen ALC; Wang A; Zou S; Zhang JZ, Near-Infrared Light Absorbing Silver-Coated Hollow Gold Nanostars for Surface-Enhanced Raman Scattering Detection of Bovine Serum Albumin Using Capping Ligand Exchange. The Journal of Physical Chemistry C 2022, 126 (2), 1026–1035.
31. Kuttner C; Piotto V; Liz-Marzán LM, Plasmonic Gradient Arrays for Rapid Screening of Surface-Enhanced Raman Scattering Efficiency: Particle Libraries of Gold Nanostars. Chemistry of Materials 2021, 33 (22), 8904–8914.
32. Rodríguez-Lorenzo L; Álvarez-Puebla RA; de Abajo FJG; Liz-Marzán LM, Surface Enhanced Raman Scattering Using Star-Shaped Gold Colloidal Nanoparticles. The Journal of Physical Chemistry C 2010, 114 (16), 7336–7340.

33. Atta S; Tsoulos TV; Fabris L, Shaping Gold Nanostar Electric Fields for Surface-Enhanced Raman Spectroscopy Enhancement via Silica Coating and Selective Etching. The Journal of Physical Chemistry C 2016, 120 (37), 20749–20758.
34. Chandra K; Culver KSB; Werner SE; Lee RC; Odom TW, Manipulating the Anisotropic Structure of Gold Nanostars using Good's Buffers. Chemistry of Materials 2016, 28 (18), 6763–6769.
35. Barbosa S; Agrawal A; Rodríguez-Lorenzo L; Pastoriza-Santos I; Alvarez-Puebla RA; Kornowski A; Weller H; Liz-Marzán LM, Tuning Size and Sensing Properties in Colloidal Gold Nanostars. Langmuir 2010, 26 (18), 14943–14950. [PubMed: 20804155]
36. Pazos-Perez N; Guerrini L; Alvarez-Puebla RA, Plasmon Tunability of Gold Nanostars at the Tip Apexes. ACS Omega 2018, 3 (12), 17173–17179. [PubMed: 31458336]
37. M. Pallares R; Stilson T; Choo P; Hu J; Odom TW, Using Good's Buffers To Control the Anisotropic Structure and Optical Properties of Spiky Gold Nanoparticles for Refractive Index Sensing. ACS Applied Nano Materials 2019, 2 (8), 5266–5271.
38. Siegel AL; Baker GA, Bespoke nanostars: synthetic strategies, tactics, and uses of tailored branched gold nanoparticles. Nanoscale Advances 2021, 3 (14), 3980–4004. [PubMed: 36132836]
39. Atta S; Pennington AM; Celik FE; Fabris L, TiO2 on Gold Nanostars Enhances Photocatalytic Water Reduction in the Near-Infrared Regime. Chem 2018, 4 (9), 2140–2153.
40. Atta S; Celik FE; Fabris L, Enhancing hot electron generation and injection in the near infrared via rational design and controlled synthesis of TiO2–gold nanostructures. Faraday Discussions 2019, 214 (0), 341–351. [PubMed: 30843543]
41. Atta S; Beetz M; Fabris L, Understanding the role of AgNO3 concentration and seed morphology in the achievement of tunable shape control in gold nanostars. Nanoscale 2019, 11 (6), 2946–2958. [PubMed: 30693922]
42. Wang H-N; Crawford BM; Fales AM; Bowie ML; Seewaldt VL; Vo-Dinh T, Multiplexed Detection of MicroRNA Biomarkers Using SERS-Based Inverse Molecular Sentinel (iMS) Nanoprobes. The Journal of Physical Chemistry C 2016, 120 (37), 21047–21055.
43. Ngo HT; Gandra N; Fales AM; Taylor SM; Vo-Dinh T, Sensitive DNA detection and SNP discrimination using ultrabright SERS nanorattles and magnetic beads for malaria diagnostics. Biosensors and Bioelectronics 2016, 81, 8–14. [PubMed: 26913502]
44. Niu W; Chua YAA; Zhang W; Huang H; Lu X, Highly Symmetric Gold Nanostars: Crystallographic Control and Surface-Enhanced Raman Scattering Property. Journal of the American Chemical Society 2015, 137 (33), 10460–10463. [PubMed: 26259023]
45. Jimenez de Aberasturi D; Serrano-Montes AB; Langer J; Henriksen-Lacey M; Parak WJ; Liz-Marzán LM, Surface Enhanced Raman Scattering Encoded Gold Nanostars for Multiplexed Cell Discrimination. Chemistry of Materials 2016, 28 (18), 6779–6790.
46. Khoury CG; Vo-Dinh T, Gold Nanostars For Surface-Enhanced Raman Scattering: Synthesis, Characterization and Optimization. The Journal of Physical Chemistry C 2008, 112 (48), 18849–18859.
47. Yuan H; Khoury CG; Hwang H; Wilson CM; Grant GA; Vo-Dinh T, Gold nanostars: surfactant-free synthesis, 3D modelling, and two-photon photoluminescence imaging. Nanotechnology 2012, 23 (7), 075102. [PubMed: 22260928]
48. De Silva Indrasekara AS; Johnson SF; Odion RA; Vo-Dinh T, Manipulation of the Geometry and Modulation of the Optical Response of Surfactant-Free Gold Nanostars: A Systematic Bottom-Up Synthesis. ACS Omega 2018, 3 (2), 2202–2210. [PubMed: 29503975]
49. Wu H-L; Chen C-H; Huang MH, Seed-Mediated Synthesis of Branched Gold Nanocrystals Derived from the Side Growth of Pentagonal Bipyramids and the Formation of Gold Nanostars. Chemistry of Materials 2009, 21 (1), 110–114.
50. Pu Y; Zhao Y; Zheng P; Li M, Elucidating the Growth Mechanism of Plasmonic Gold Nanostars with Tunable Optical and Photothermal Properties. Inorganic Chemistry 2018, 57 (14), 8599–8607. [PubMed: 29953211]
51. Atta S; Rangan S; Fabris L, Highly Tunable Growth and Etching of Silica Shells on Surfactant-Free Gold Nanostars. ChemNanoMat 2020, 6 (1), 53–57.

52. Fabris L; Indrasekara S; Atta S, Interface Engineering of Gold Nanostars for Biomedical Applications. In World Scientific Reference on Plasmonic Nanomaterials, World Scientific: 2021; Vol. Volume 22, pp 21–71.

53. Tsoulos TV; Atta S; Lagos MJ; Beetz M; Batson PE; Tsilomelekis G; Fabris L, Colloidal plasmonic nanostar antennas with wide range resonance tunability. Nanoscale 2019, 11 (40), 18662–18671. [PubMed: 31584591]

54. Yuan H; Liu Y; Fales AM; Li YL; Liu J; Vo-Dinh T, Quantitative Surface-Enhanced Resonant Raman Scattering Multiplexing of Biocompatible Gold Nanostars for in Vitro and ex Vivo Detection. Analytical Chemistry 2013, 85 (1), 208–212. [PubMed: 23194068]

55. Xie Y; Chen T; Cheng Y; Wang H; Qian H; Yao W, SiO2@Au nanoshells-based SERS method for detection of sunset yellow and chrysoidine. Spectrochimica Acta Part A: Molecular and Biomolecular Spectroscopy 2014, 132, 355–360. [PubMed: 24880685]

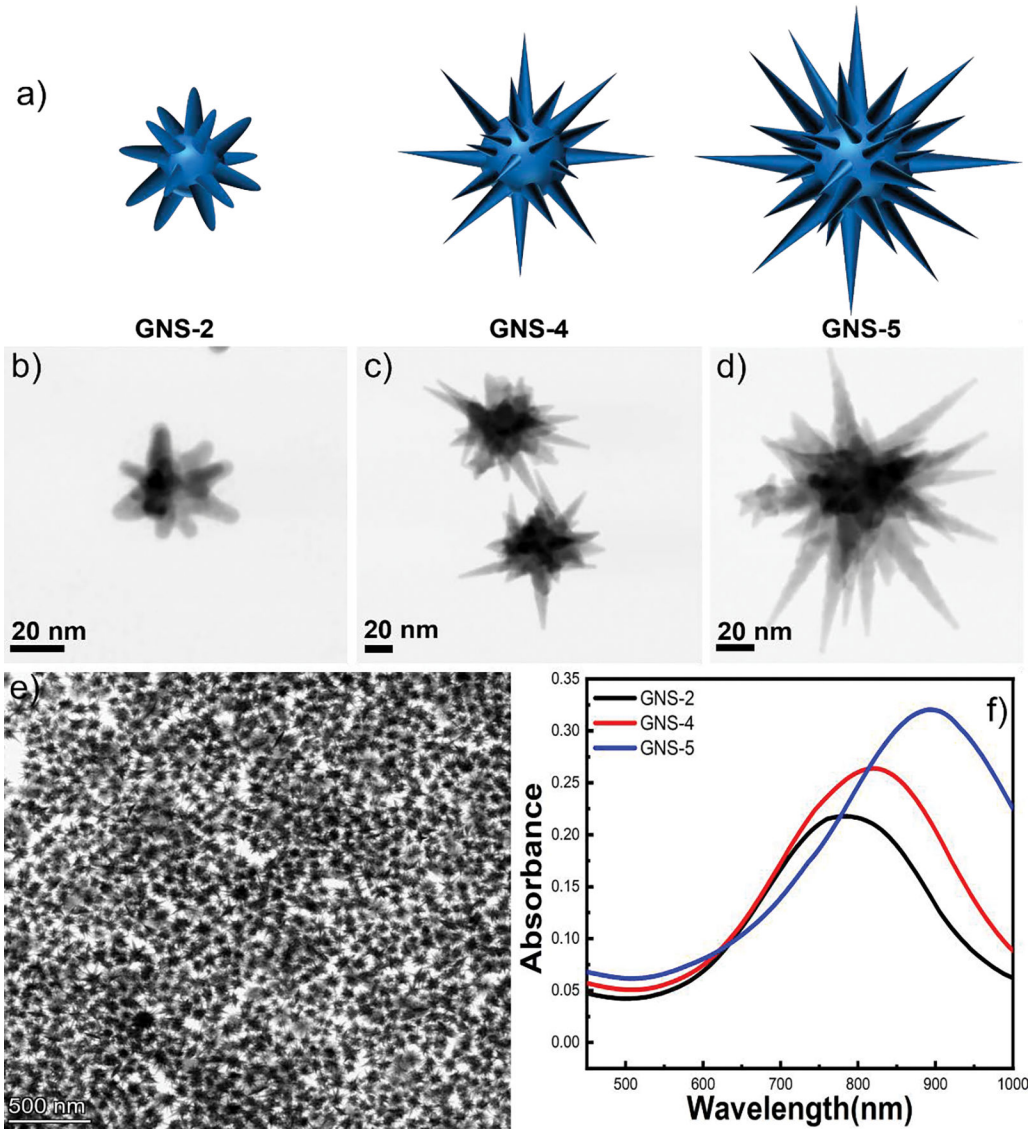

Figure 1.

3D model of GNS-2, GNS-4, and GNS-5 morphology (a). TEM image of GNS-2 (b), GNS-4 (c) and GNS-5 (d). TEM image having multiple nanostars of GNS-5 showing high monodispersity of the synthesis (e). UV-vis spectra of GNS-2, GNS-4, and GNS-5 morphology showing a red shift from 780 nm to 890 nm when the GNS morphology changes from GNS-2 to GNS-5 (f).

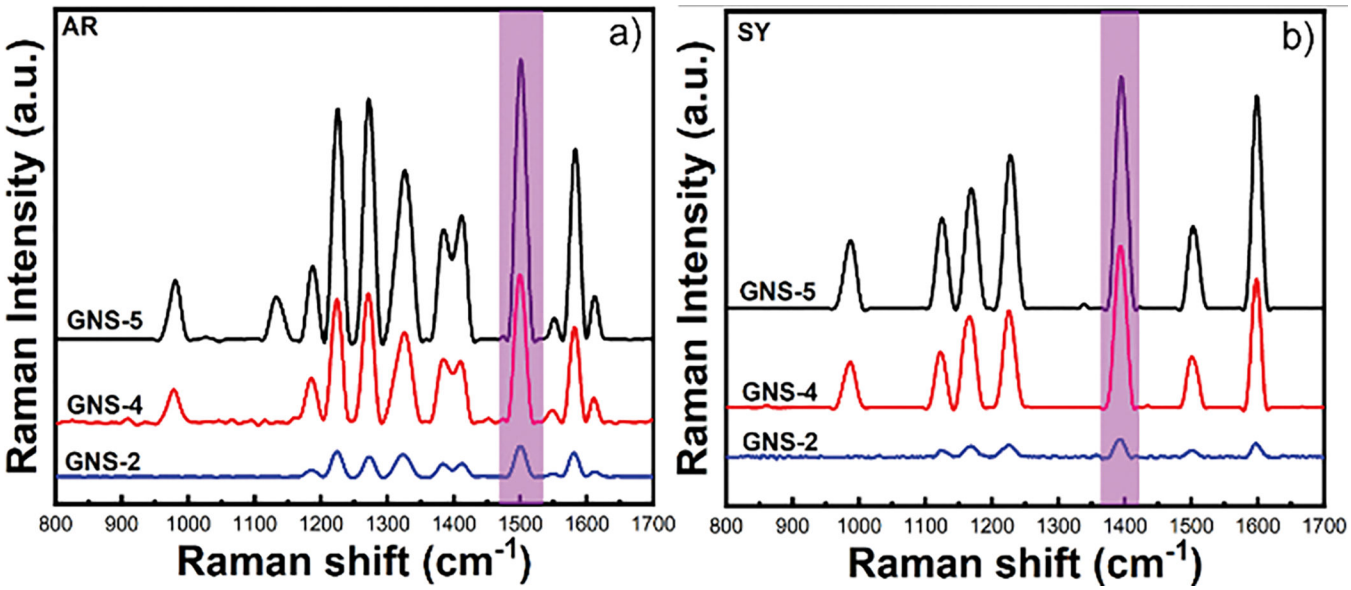

Figure 2.

Comparison of SERS signal intensity of allura red dye using GNS-2, GNS-4, and GNS-5 (a). Comparison of SERS signal intensity of sunset yellow with GNS-2, GNS-4, and GNS-5 (b).

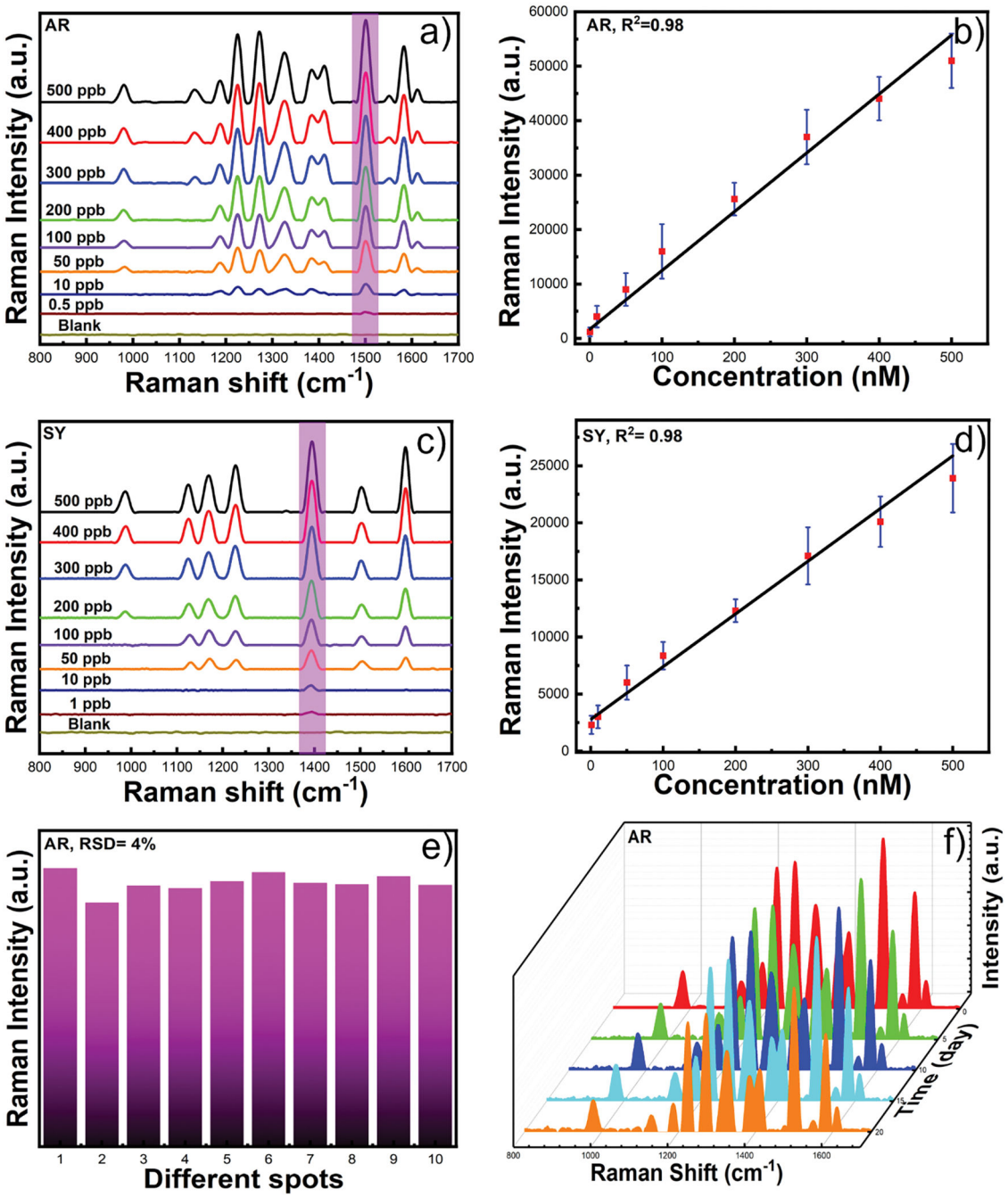

Figure 3.

SERS spectra of AR using GNS-5 at different concentrations from 500 ppb to 0.5 ppb (a). The calibration curve for the characteristic peak intensity at 1500 cm^{-1} as a function of AR concentration (b). SERS spectra of SY at different concentration from 500 ppb to 1 ppb (c) and SERS intensity of SY at 1395 cm^{-1} as a function of different concentrations (d). SERS reproducibility of allura red using GNS-5 (e). Representative SERS spectra of GNS-5 after 20 days measured with 5 days interval showing good stability of GNS-5(f).

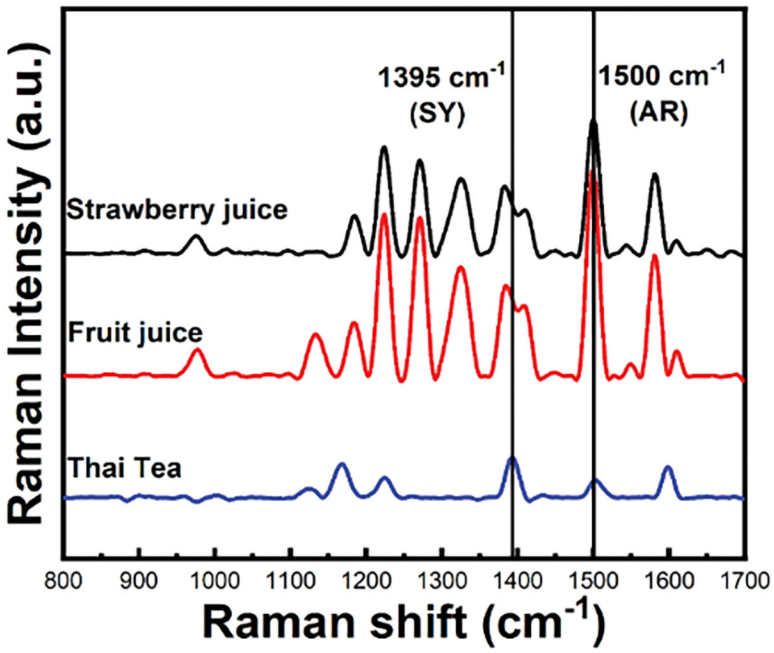

Figure 4.
Representative SERS spectra of beverages where GNS-5 was utilized as a SERS probe.

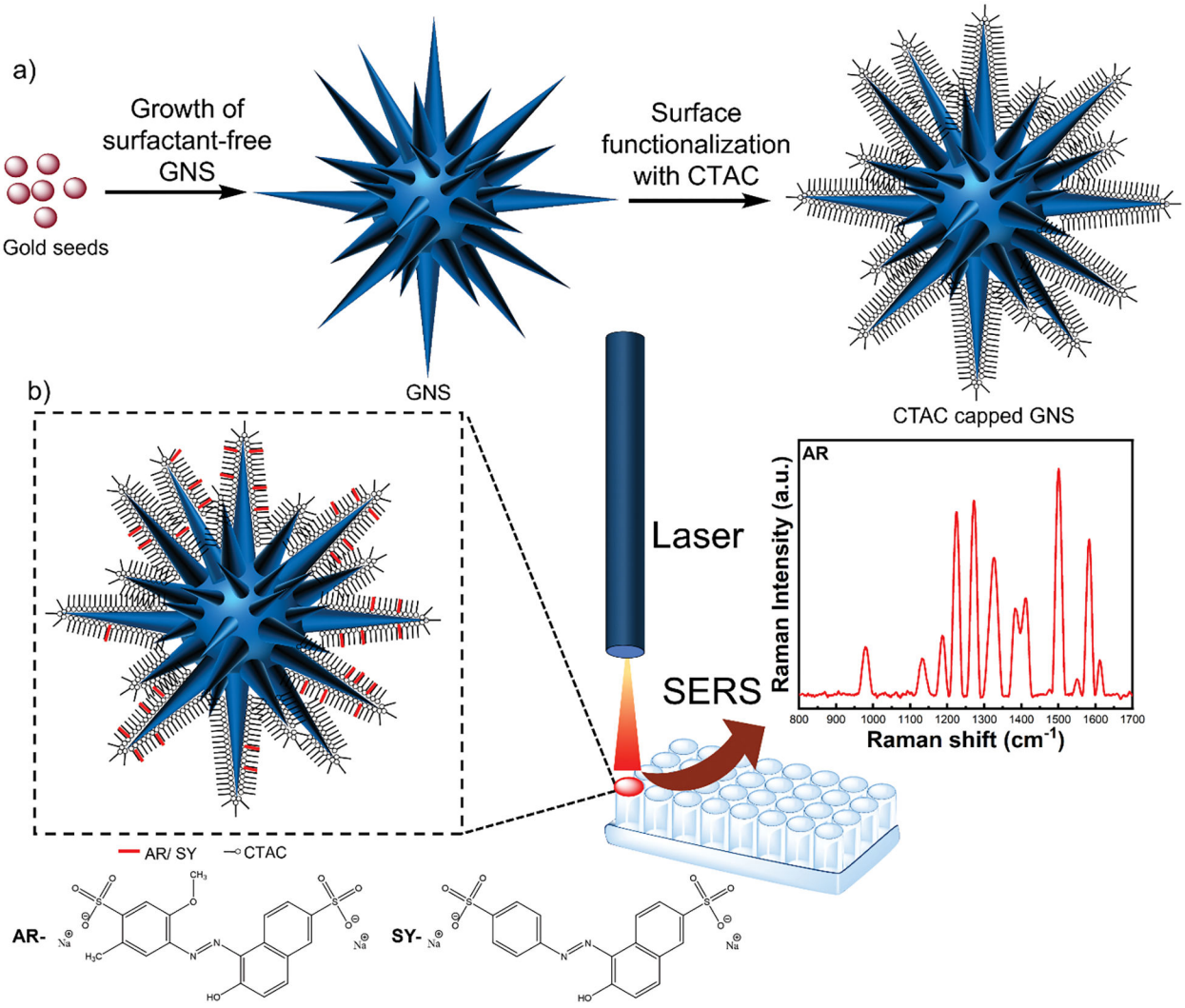

Scheme 1.

Schematic of the synthetic procedure of CTAC capped GNS-5 where the GNS-5 morphology was achieved by systematic controlling of the concentrations of reagents including gold salt, HCl, ascorbic acid, and $AgNO_3$ (a), and a simple procedure for SERS detection of weak-affinity analytes which involves simple mixing of analytes in a well plate having CTAC capped GNS-5 (b).

Table 1.

Morphological characterization of GNS-2, GNS-4, and GNS-5.

	Number of spikes	Core size (nm)	Spike length (nm)	Spike aspect ratio	Spike sharpness
GNS-2	7–8	22 ± 10	18 ± 8	1.8	7 ± 2
GNS-4	10–15	40 ± 20	45 ± 8	4	3 ± 2
GNS-5	20–35	50 ± 20	53 ± 12	5.2	3 ± 2